ChemComm

COMMUNICATION

View Article Online
View Journal | View Issue

Cite this: *Chem. Commun.*, 2026, **62**, 6721

Received 20th January 2026,
Accepted 25th February 2026

DOI: 10.1039/d6cc00368k

rsc.li/chemcomm

High-pressure crystal structure and phase transitions in B_2O_3

Dominik Spahr, *[a] Sean S. Sebastian,[b] Lukas Brüning,[b] Pascal L. Jurzick,[b] Ninel Sharapova,[b] Lkhamsuren Bayarjargal,[a] Elena Bykova,[a] Maxim Bykov,[b] Victor Milman[c] and Björn Winkler[a]

A high-pressure polymorph of boron oxide, B_2O_3-$P2_12_12_1$, has been obtained in a laser-heated diamond anvil cell at 50(3) GPa after heating boron trioxide to a temperature of $T_{max} \leq 2500(300)$ K. The crystal structure was determined from synchrotron single crystal X-ray diffraction and was confirmed by a combination of density functional theory (DFT) calculations and experimental Raman spectroscopy. Experimental- as well as DFT-data confirm the non-centrosymmetric/non-polar space group $P2_12_12_1$. The structural model of B_2O_3-$P2_12_12_1$ is in agreement with an earlier DFT-based crystal structure prediction. The crystal structure is characterized by corner-sharing [BO_4] tetrahedra with covalent B–O bonds. Our experimental Raman data show that B_2O_3-$P2_12_12_1$ can be recovered under ambient conditions.

In the context of studies aimed at rationalizing the formation of chemically simple carbonates of small cations (*e.g.* Be^{2+}, Al^{3+}, and Fe^{3+}),[1–4] we attempted to synthesize a borocarbonate by reacting B_2O_3 with CO_2 at moderate pressures in a laser heated diamond anvil cell (LH-DAC).[5] Due to co-condensation of H_2O in the sample chamber of the DAC, the reaction product was a hydrous borocarbonate B[μ-H(CO_3)$_2$], obtained at ≈20 GPa and ≈1500(200) K.[5] Here, we therefore repeated the experiment, aiming at the synthesis of an anhydrous borocarbonate. Employing an improved cryogenic loading system, which reduces the H_2O contamination,[6] we searched for reactions in the B_2O_3–CO_2 system between 20 GPa and 50 GPa. This search was motivated by the fact that compounds containing boron oxoanions are a rich class of optical materials, which are employed in numerous applications.[7–11] Although no reaction between B_2O_3 and CO_2 was detected, we observed the formation of a new high pressure polymorph of B_2O_3.

The present study therefore complements and significantly extends the numerous previous high-pressure studies of B_2O_3. B_2O_3 is a rare example where the structure of a high-pressure polymorph (B_2O_3-$Ccm2_1$)[12] was determined before the structure of the likely ground state structure (B_2O_3-$P3_121$) had been correctly determined.[13,14] The high-pressure B_2O_3 polymorph crystallizes in the non-centrosymmetric space group $Ccm2_1$ and was described in the non-default representations of space group *Cmc*21 (No. 36).[12] The experimentally challenging determination of the ambient pressure phase of B_2O_3-$P3_121$ is due to the extreme difficulties encountered when attempting to crystallize samples from melts, as B_2O_3 is an outstanding glass former, and is also hygroscopic. Hence, B_2O_3 glasses have been studied in detail.[15] While the earlier diffraction studies[16–19] were therefore revised later, it was, correctly, inferred at an early stage that B_2O_3-$P3_121$ transformed into a new polymorph at pressures above 2.5 GPa.[20] The stability field of the high pressure polymorph B_2O_3-$Ccm2_1$ has been discussed in several studies and is now well established up to 8 GPa and 1800 K.[20–23] An equation of state based on compression data up to 42 GPa was determined by Nieto-Sanz *et al.*[24] Refitting their data to a third-order Birch–Murnaghan equation of state[25–27] gives a bulk modulus of 160(17) GPa (with K_p = 3.1(7) GPa).

There have been several atomistic modeling and crystal structure prediction studies. Li *et al.*[28] carried out DFT-LDA calculations to understand the band gaps and some physical properties of B_2O_3-$P3_121$ and B_2O_3-$Ccm2_1$, while Takeda *et al.*[29] studied the structures of the two polymorphs with a Hartree–Fock-based approach. Dong *et al.*[30] used a crystal structure prediction approach to search for hard oxides and predicted a phase transition from B_2O_3-$Ccm2_1$ to B_2O_3-$P2_12_12_1$ at 46 GPa in the athermal limit. In contrast, another recent structure prediction study[31] predicted B_2O_3-structures with space group symmetries of *Pbcn* at 15 GPa, *P*1 at 25 GPa, and *C*2/*c* at 50 GPa.

In our experiments, the B_2O_3 powder was first dried in an oven at ≈580 K and then placed in the sample chamber of the DAC. Afterwards, CO_2-I (dry ice) was added by cryogenic loading into the sample chamber (see the SI). In the last step, the DAC

[a] *Goethe University Frankfurt, Institute of Geosciences, Altenhöferallee 1, Frankfurt 60438, Germany. E-mail: d.spahr@kristall.uni-frankfurt.de*
[b] *Goethe University Frankfurt, Institute of Inorganic and Analytical Chemistry, Max-von-Laue-Straße 7, Frankfurt 60438, Germany*
[c] *Dassault Systèmes BIOVIA, 22 Cambridge Science Park, CB4 0FJ, Cambridge, UK*

was closed and compressed to the target pressure of the experiment. Using Raman spectroscopy, we excluded any contamination with H_2O, due to the absence of characteristic Raman modes of H_2O-VII after the cryogenic loading at high wave numbers ($\approx$3000–3400 cm^{-1}).[32,33] In addition, we confirmed by Raman spectroscopy that CO_2-I ($Pa\bar{3}$) is present in the sample chamber.[34,35] During cold compression, CO_2-I undergoes a phase transition to phase III (*Cmca*) in a broad ($\approx$5 GPa) pressure range around $\approx$12 GPa and persists in a meta-stable state up to high pressures.[34–36] Heating CO_2-III at pressures above $\approx$25 GPa causes another phase transformation to phase V ($I4\bar{2}d$), which is the stable CO_2-polymorph up to pressures >100 GPa.[36,37] In B_2O_3, a phase transition from B_2O_3-$P3_121$ to B_2O_3-$Ccm2_1$ was observed in earlier studies above 2–6 GPa, depending on temperature.[20–23]

Heating B_2O_3 in the CO_2 environment between 20 GPa and 40 GPa up to maximum temperatures of $T_{max} \leq$ 2500(300) K did not result in the formation of a new carbonate, which can typically be identified by Raman bands due to the C–O stretching vibration. However, after laser heating ($T_{max} \leq$ 2500(300) K) B_2O_3 at 50(3) GPa for 30 minutes (Fig. 1a), we observed, in addition to the characteristic Raman modes of B_2O_3-$Ccm2_1$, the appearance of new Raman modes. The experimental Raman spectrum of B_2O_3-$Ccm2_1$ is accurately reproduced by our DFT-based calculations (Fig. 2b), and hence the Raman bands belonging to the new phase can clearly be identified. Employing spatially resolved Raman spectroscopy we found that the unknown phase with a strong Raman mode at $\approx$280 cm^{-1} (Fig. 2c) is present on one side of the heated B_2O_3 grain (Fig. 1b and f). The other part of the sample shows the Raman signal of B_2O_3-$Ccm2_1$ (Fig. 1b and e) with a dominant Raman mode at $\approx$470 cm^{-1}. Around the heated B_2O_3 sample, we could only detect the Raman signature of CO_2-V, which can be identified in a straightforward fashion as the experimental Raman spectrum of CO_2-V is in good agreement with our DFT-based calculations (Fig. 2a). In the unheated areas of the DAC, metastable CO_2-III is still present (Fig. 1b).

We solved the crystal structure of the unknown phase, using synchrotron-based single crystal X-ray diffraction, in the orthorhombic acentric space group $P2_12_12_1$ with Z = 4 and B_2O_3 composition (Fig. 3a). The lattice parameters at 50(3) GPa are a = 4.1372(4) Å, b = 7.351(1) Å and c = 3.9417(6) Å (V = 119.88(3) Å^3). The very low R_1-value (3.7%), in combination with a reasonable reflection-to-parameter-ratio (6.9 : 1) for a DAC-experiment, is indicative of a good structure refinement. The displacement parameters of all atoms were refined anisotropically and no constraints or restraints were introduced. This structural model had been predicted by an evolutionary algorithm in the B–O binary system, with a proposed stability field of 46–133 GPa in the athermal limit.[30] Our DFT-based full geometry optimizations on B_2O_3-$P2_12_12_1$ accurately reproduce our experimental

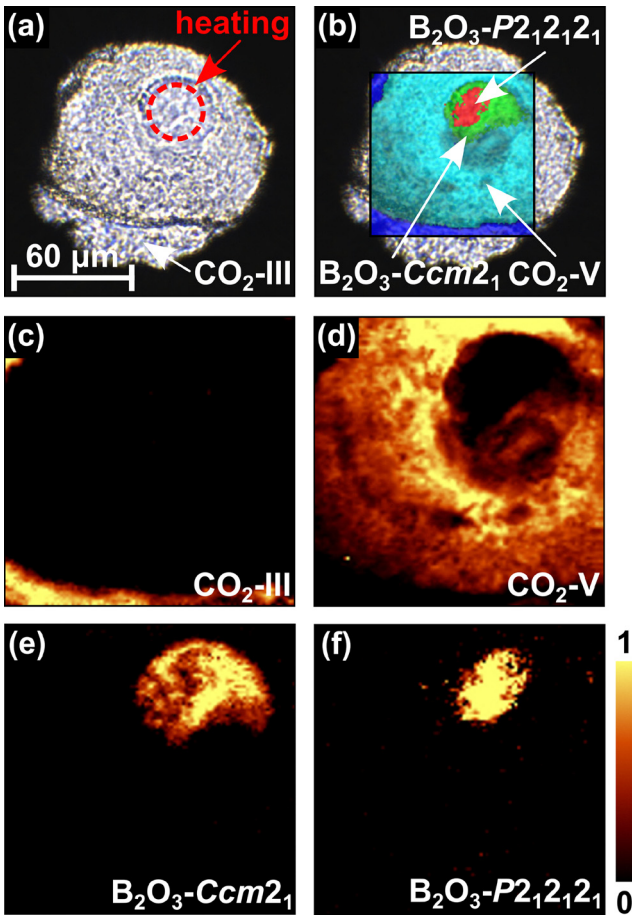

Fig. 1 (a) B_2O_3 grain in a CO_2 atmosphere at 50(3) GPa after laser heating ($T_{max} \leq$ 2500(300) K). (b) Combined Raman maps of B_2O_3-$P2_12_12_1$, B_2O_3-$Ccm2_1$, CO_2-V and CO_2-III after laser heating overlaid on a picture of the sample chamber. Raman maps of: (c) CO_2-III ($\approx$370 cm^{-1}), (d) CO_2-V ($\approx$800 cm^{-1}), (e) B_2O_3-$Ccm2_1$ ($\approx$470 cm^{-1}) and (f) B_2O_3-$P2_12_12_1$ ($\approx$280 cm^{-1}) after laser heating at 50(3) GPa.

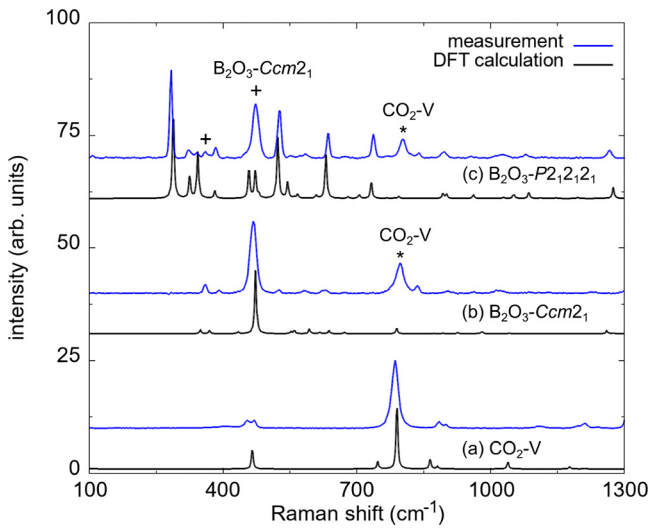

Fig. 2 Raman spectroscopy at 50(3) GPa after laser heating: (a) Raman spectra of CO_2–V. (b) Raman spectra of B_2O_3-$Ccm2_1$. (c) Raman spectra of B_2O_3-$P2_12_12_1$. Experimental Raman spectra are shown in blue, and DFT-based calculations are shown in black. The Raman shifts of the theoretical spectra were scaled by 1–3%. Peaks of CO_2–V in the Raman spectra of B_2O_3 are marked with an asterisk (*). Peaks of B_2O_3-$Ccm2_1$ in the Raman spectra of B_2O_3-$P2_12_12_1$ are marked with a cross (+).

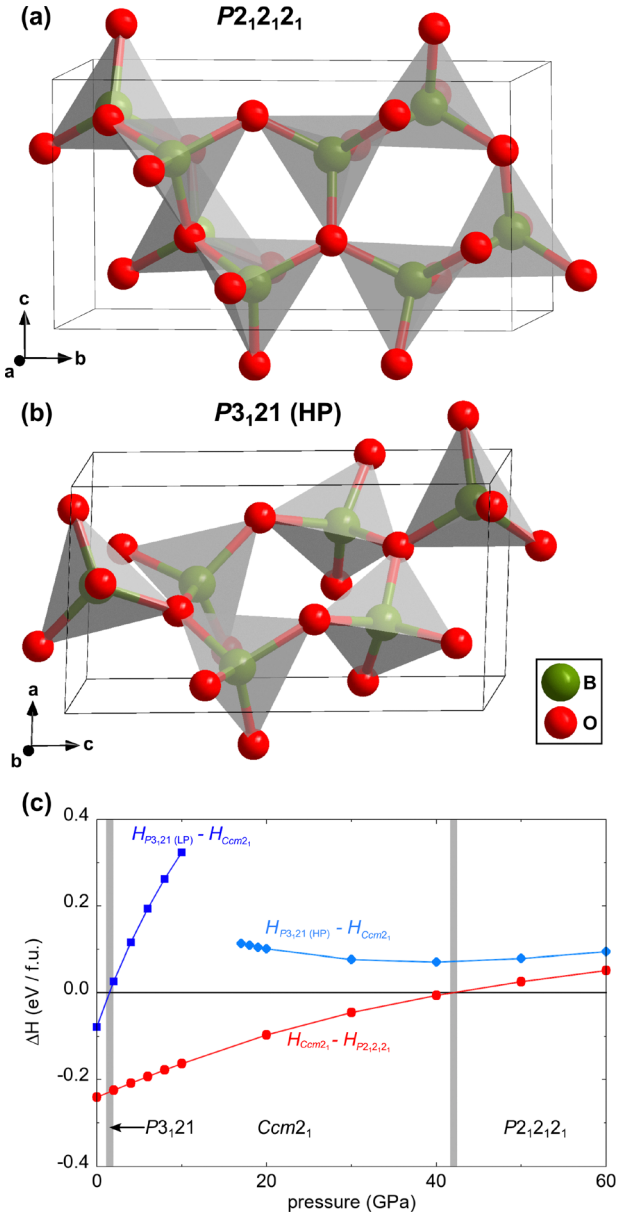

Fig. 3 (a) Crystal structure of B_2O_3-$P2_12_12_1$ obtained from synchrotron single-crystal X-ray diffraction at 50(3) GPa. (b) Crystal structure of B_2O_3-$P3_121$ (HP) obtained from DFT-based calculations at 50 GPa. (c) Enthalpy difference (ΔH) between different B_2O_3 phases for the pressure range 0–60 GPa from DFT-based calculations.[12,13,30]

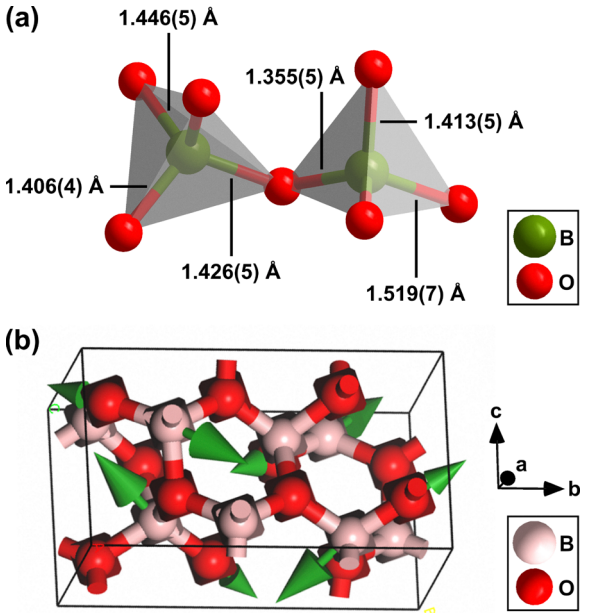

Fig. 4 (a) Geometry of two [BO_4] tetrahedra in the crystal structure of B_2O_3-$P2_12_12_1$ from single crystal structure refinement at 50(3) GPa. (b) Eigenvector of the atomic displacements in B_2O_3-$P2_12_12_1$ for the characteristic Raman mode at ≈1332 cm^{-1} from DFPT calculations.

structural model and the earlier structure prediction (Table S1 in the SI).[30] Hence, our single crystal X-ray diffraction data clearly show that no reaction between B_2O_3 and CO_2 had occurred.

The structure of B_2O_3-$P2_12_12_1$ is characterized by interconnected [BO_4] tetrahedra (Fig. 3a) with B–O bond lengths between 1.355(5) Å and 1.519(7) Å at 50(3) GPa. The experimental B–O bond lengths are in agreement with our DFT calculations (1.35–1.46 Å). In the crystal structure of B_2O_3-$P2_12_12_1$, two symmetrically independent boron atoms are present, each within a [BO_4] tetrahedron (Fig. 4a). Each of the [BO_4] tetrahedra is connected by corner-sharing to the neighboring tetrahedra (Fig. 3a and 4a). Two of the symmetrically independent oxygen atoms form bonds to three boron atoms of other tetrahedra. The last independent oxygen atom forms only two B–O contacts, which are noticeably shorter than other B–O bonds in the crystal structure. A Mulliken population analysis yielded noticeably stronger bonds for the shortest B–O bonds (0.87 e^- $Å^{-3}$) than for the longest B–O bonds (0.58 e^- $Å^{-3}$). All B–O bonds show a significantly covalent character. The B–O bond length (1.35–1.48 Å) and the bond populations (0.79–0.57 e^- $Å^{-3}$) are in agreement with our DFT-based calculations for the [BO_4] tetrahedra in B_2O_3-$Ccm2_1$ at 50 GPa.

We employed DFPT-based calculations in order to derive a theoretical Raman spectrum of B_2O_3-$P2_12_12_1$ at 50 GPa. Our experimental Raman spectrum is in reasonable agreement with the theoretical one. For several Raman modes, the calculated Raman intensities differ noticeably from the experimental data (Fig. 2c). This can be rationalized by noting that we computed the Raman spectrum for an ideal powder, while experimentally we record the spectrum of very few grains with unknown orientation. An analysis of the eigenvectors shows that the characteristic Raman bands are due to complex displacement patterns, which generally defy a straightforward simple classification. An exception is the mode at 1332 cm^{-1} (Fig. 4b), which is due to an asymmetric stretching vibration of the [BO_4] tetrahedra.

We computed the p,V-relations for all three polymorphs and fitted the equation of states (EoS) to these data (Fig. S2 in the SI). We also computed the elastic stiffness tensors for all three polymorphs (Table S3 in the SI). As expected, the bulk modulus from the EoS calculations increases from 41.0(9) GPa for B_2O_3-$P3_121$ to 145(4) GPa for B_2O_3-$Ccm2_1$ to 157(1) GPa for B_2O_3-

$P2_12_12_1$. The corresponding values from the stress–strain calculations agree with these values within a few GPa (see the SI). Our results are consistent with the data reported by Dong *et al.*[30] From our DFT calculations, we also found that another B_2O_3 polymorph may be formed metastably at elevated pressures. The ambient pressure phase B_2O_3-$P3_121$ (LP) undergoes an isostructural phase transition to B_2O_3-$P3_121$ (HP) at $\approx$17 GPa (Fig. 3b). This phase transition is accompanied by a significant volume decrease of $\approx$10% within 1 GPa and a change of the boron coordination from trigonal-planar [BO_3] units to [BO_4] tetrahedra (Table S4 in the SI). The bulk modulus of this new high-pressure phase is significantly higher (K_0 = 202(1) GPa with K_p = 3.70(4)) than calculated for the other two high-pressure polymorphs. A comparison of the enthalpies of all four B_2O_3 phases between ambient pressure and 60 GPa (Fig. 3c) shows that B_2O_3-$P3_121$ (LP) is less stable than B_2O_3-$Ccm2_1$ at pressures $>$1.5 GPa. B_2O_3-$Ccm2_1$ remains stable up to 42 GPa and undergoes a phase transition to B_2O_3-$P2_12_12_1$. These results are consistent with the earlier work by Dong *et al.*[30] predicting the phase transitions at similar pressures. The metastable polymorph B_2O_3-$P3_121$ (HP) is less stable by $\approx$0.1 eV f.u.$^{-1}$ with respect to B_2O_3-$Ccm2_1$ at 17 GPa. Hence, we assume that this phase may be found experimentally by careful cold-compression of B_2O_3-$P3_121$ (LP) in a hydrostatic pressure transmitting medium (*e.g.* helium).

We also computed the phonon dispersion curves of B_2O_3-$P2_12_12_1$ at 50 GPa and at ambient pressures (Fig. S4 in the SI). In agreement with the experimental observations, B_2O_3-$P2_12_12_1$ is dynamically stable at 50 GPa in the athermal limit. Hence, we measured Raman spectroscopy during decompression in order to understand if B_2O_3-$P2_12_12_1$ can be recovered under ambient conditions. Our experimental Raman data clearly show that the characteristic Raman modes of both B_2O_3-$P2_12_12_1$ and B_2O_3-$Ccm2_1$ are still present after opening the DAC (Fig. S3 in the SI). They are in agreement with our Raman spectra obtained from the DFPT-calculations, confirming that both phases can be recovered under ambient conditions. This is in agreement with our phonon dispersion curves at ambient pressures, which show that B_2O_3-$P2_12_12_1$ is dynamically stable at the athermal limit (Fig. S4 in the SI).

In conclusion, we have obtained the boron trioxide polymorph B_2O_3-$P2_12_12_1$ in a LH-DAC at 50(3) GPa, which crystalizes in a non-centrosymmetric/non-polar space group. B_2O_3-$P2_12_12_1$ was obtained by heating up to a maximum temperature of $T_{max} \leq$ 2500(300) K. We determined the crystal structure by synchrotron single crystal X-ray diffraction and corroborated the structural model by a combination of experimental Raman spectroscopy and DFT-based calculations. Its acentric orthorhombic crystal structure is in agreement with the results from an earlier crystal structure prediction,[30] while the predicted structures in another study[31] were not obtained. Our experimental data show that B_2O_3-$P2_12_12_1$ can be recovered under ambient conditions next to the well-established high-pressure polymorph B_2O_3-$Ccm2_1$.[12] Our results show that B_2O_3 does not react with CO_2 at elevated pressures and temperatures. This is in contrast to other chemically simple oxides such as Al_2O_3, Fe_2O_3, Cr_2O_3 or I_2O_5, which readily form carbonates when heated in a CO_2 environment.[3,4,6,38]

Conflicts of interest

There are no conflicts to declare.

Data availability

All study data are included in the article and/or in the supplementary information (SI). Supplementary information: experimental and computational details, crystallographic data, X-ray single crystal measurements, Raman spectroscopy and DFT-based calculations. See DOI: https://doi.org/10.1039/d6cc00368k.

CCDC 2523450 contains the supplementary crystallographic data for this paper.[39]

Acknowledgements

We gratefully acknowledge funding from the DFG (WI1232 and BA4020) and the DFG Emmy-Noether Program (projects BY101/2-1 and BY112/2-1). E. B. and M. B. acknowledge the support from the Johanna-Quandt-Stiftung. M. B. acknowledges the support from the LOEWE program. B. W. is grateful for the support from the Dassault Systèmes Science Ambassador program. P. L. J. acknowledges funding from the Studienstiftung des deutschen Volkes. We acknowledge the European Synchrotron Radiation Facility (ESRF) for provision of synchrotron radiation facilities under proposal number CH-7616, and we would like to thank Jon Wright for assistance and support in using beamline ID11 (doi: https://doi.org/10.15151/ESRF-ES-2241566191).

References

1 D. Spahr, L. Bayarjargal, E. Bykova, M. Bykov, T. H. Reuter, L. Brüning, P. L. Jurzick, L. Wedek, V. Milman, B. Wehinger and B. Winkler, *Chem. Commun.*, 2024, **60**, 10208–10211.
2 D. Spahr, L. Bayarjargal, E. Bykova, M. Bykov, L. Brüning, V. Kovalev, V. Milman, J. Wright and B. Winkler, *Inorg. Chem.*, 2024, **63**, 19513–19517.
3 L. Bayarjargal, D. Spahr, V. Milman, J. Marquardt, N. Giordano and B. Winkler, *Inorg. Chem.*, 2023, **62**, 13910–13918.
4 L. Bayarjargal, D. Spahr, E. Bykova, Y. Wang, N. Giordano, V. Milman and B. Winkler, *Inorg. Chem.*, 2024, **63**, 21637–21644.
5 D. Spahr, T. H. Reuter, E. Bykova, L. Bayarjargal, L. Brüning, V. Kovalev, L. Wedek, V. Milman, J. Wright and B. Winkler, *Inorg. Chem.*, 2025, **64**, 19146–19150.
6 D. Spahr, L. Bayarjargal, L. Brüning, V. Kovalev, E. Bykova, M. Bykov, V. Milman, M. Mezouar and B. Winkler, *JACS Au*, 2025, **5**, 4675–4680.
7 M. Mutailipu, K. R. Poeppelmeier and S. Pan, *Chem. Rev.*, 2021, **121**, 1130–1202.
8 P. Becker, *Adv. Mater.*, 1998, **10**, 979–992.
9 C. T. Chen and G. Z. Liu, *Annu. Rev. Mater. Sci.*, 1986, **16**, 203–243.
10 M. Mutailipu, M. Zhang, Z. H. Yang and S. L. Pan, *Acc. Chem. Res.*, 2019, **52**, 791–801.
11 T. Sasaki, Y. Mori, M. Yoshimura, Y. K. Yap and T. Kamimura, *Mater. Sci. Eng., R*, 2000, **30**, 1–54.
12 C. T. Prewitt and R. D. Shannon, *Acta Crystallogr. B*, 1968, **24**, 869–874.
13 H. Effenberger, C. Lengauer and E. Parthé, *Monatsh. Chem.*, 2001, **132**, 1515–1517.

14 M. Burianek, J. Birkenstock, P. Mair, V. Kahlenberg, O. Medenbach, R. D. Shannon and R. X. Fischer, *Phys. Chem. Min.*, 2016, **43**, 527–534.
15 A. C. Wright, *Phys. Chem. Glasses: Eur. J. Glass Sci. Technol., Part B*, 2018, **59**, 65–87.
16 S. V. Berger, *Acta Crystallogr.*, 1952, **5**, 389.
17 S. V. Berger, *Acta Chem. Scand.*, 1953, **7**, 611–622.
18 S. L. Strong and R. Kaplow, *Acta Crystallogr. B*, 1968, **24**, 1032–1036.
19 G. E. Gurr, P. W. Montgomery, C. D. Knutson and B. T. Gorres, *Acta Crystallogr. B*, 1970, **26**, 906–915.
20 F. Dachille and R. Roy, *J. Am. Ceram. Soc.*, 1970, **42**, 78–80.
21 J. D. Mackenzie and W. F. Claussen, *J. Am. Ceram. Soc.*, 1961, **44**, 79–81.
22 V. V. Brazhkin, Y. Katayama, Y. Inamura, M. V. Kondrin, A. G. Lyapin, S. V. Popova and R. N. Voloshin, *JETP Lett.*, 2003, **78**, 393–397.
23 V. L. Solozhenko, O. O. Kurakevych, Y. Le Godec and V. V. Brazhkin, *J. Phys. Chem. C*, 2015, **119**, 20600–20605.
24 D. Nieto-Sanz, P. Loubeyre, W. Crichton and M. Mezouar, *Phys. Rev. B: Condens. Matter Mater. Phys.*, 2004, **70**, 214108.
25 F. Murnaghan and Proc Natl, *Acad. Sci.*, 1944, **30**, 244–247.
26 F. Birch, *Phys. Rev.*, 1947, **71**, 809–824.
27 J. Gonzalez-Platas, M. Alvaro, F. Nestola and R. Angel, *J. Appl. Crystallogr.*, 2016, **49**, 1377–1382.
28 D. Li and W. Y. Ching, *Phys. Rev. B: Condens. Matter Mater. Phys.*, 1996, **54**, 13616.
29 A. Takada, C. R. A. Catlow, G. D. Price and C. L. Hayward, *Phys. Chem. Min.*, 1997, **24**, 423–431.
30 H. Dong, A. R. Oganov, V. V. Brazhkin, Q. Wang, J. Zhang, M. M. D. Esfahani, X.-F. Zhou, F. Wu and Q. Zhu, *Phys. Rev. B*, 2018, **98**, 174109.
31 H. Kuang, Y. Pan and J. S. Tse, *J. Phys. Chem. C*, 2024, **128**, 3543–3556.
32 P. Pruzan, J. C. Chervin and M. Gauthier, *EPL*, 1990, **13**, 81–87.
33 W.-P. Hsieh and Y.-H. Chien, *Sci. Rep.*, 2015, **5**, 8532.
34 K. Aoki, H. Yamawaki, M. Sakashita, Y. Gotoh and K. Takemura, *Science*, 1994, **263**, 356–358.
35 H. Olijnyk and A. P. Jephcoat, *Phys. Rev. B: Condens. Matter Mater. Phys.*, 1998, **57**, 879–888.
36 D. Scelta, K. F. Dziubek, M. Ende, R. Miletich, M. Mezouar, G. Garbarino and R. Bini, *Phys. Rev. Lett.*, 2021, **126**, 065701.
37 F. Datchi, B. Mallick, A. Salamat and S. Ninet, *Phys. Rev. Lett.*, 2012, **108**, 125701.
38 Y. Wang, L. Bayarjargal, M. Bykov, E. Bykova, D. Spahr, K. Glazyrin, V. Milman and B. Winkler, *Inorg. Chem.*, 2025, **64**, 4996–5003.
39 CCDC 2523450: Experimental Crystal Structure Determination, 2026, DOI: 10.5517/ccdc.csd.cc2qpvmx.